IEEE Access
Multidisciplinary | Rapid Review | Open Access Journal

Received June 16, 2019, accepted June 25, 2019, date of publication July 1, 2019, date of current version August 1, 2019.

Digital Object Identifier 10.1109/ACCESS.2019.2926140

1.4 GHz Low-Cost PIN Diode Phase Shifter for *L*-Band Radiometer Antenna

KIM TUYEN TRINH, (Student Member, IEEE), JIEWEI FENG, (Student Member, IEEE), SHAHRIAR HASAN SHEHAB, (Student Member, IEEE), AND NEMAI CHANDRA KARMAKAR, (Senior Member, IEEE)

Department of Electrical and Computer Systems Engineering, Monash University, Melbourne, VIC 3800, Australia

Corresponding author: Kim Tuyen Trinh (kim.trinh@monash.edu)

This work was supported by the Australian Research Council (ARC) under Grant DP160104233: Passive airborne radiometer for high-resolution soil moisture monitoring.

ABSTRACT A 1.4 GHz 4-bit positive intrinsic negative (PIN) diode phase shifter with compact reflective loads for an *L*-band soil moisture measuring radiometer phased array antenna has been successfully designed. Unlike conventional PIN diode phase shifters using PIN diodes as switches, the designed PIN diode phase shifter adopting the low-cost PIN diodes with poor isolation as equivalent lumped components corresponding to the forward and reverse bias states. First, the PIN diode is fully characterized for its equivalent circuit models at on- and off-states, and, then, the reflective load is designed with only one inductance in parallel with the diode models to obtain the desired phase shift. The phase shifter consists of four individual bits in cascade, providing 16 states of phase shifts. Each bit is constructed with a meander branch-line 90° coupler and two identical PIN diode reflective loads. Thus, the novel design yields a highly compact phase shifter at L-band. The phase shifter is theoretically analyzed, fabricated, and measured. The measured results show good agreement with analysis and calculations. The insertion loss of the 4-bit phase shifter is less than 2 dB within 25 MHz radiometer bandwidth and less than 2.3 dB from 1.37 to 1.43 GHz. The input and output return losses are larger than 16 dB within the 1.37 to 1.43 GHz frequency band. The root mean square (RMS) phase error is just less than 1° at the center frequency of 1.4 GHz and less than 3° within the radiometer bandwidth. The phase shifter is controlled with switching electronics and a microcontroller and integrated within the beamforming network of an L-band 4 × 4-element radiometer phased array antenna for soil moisture measurement.

INDEX TERMS Digital phase shifter, PIN diode, test-fixture, thru-reflect-line (TRL) calibration, reflection-type phase shifter, hybrid coupler, *L*-band.

I. INTRODUCTION

Water is the liquid gold of Australia, the driest continent on the earth. A single drop of water saving is crucial for the country. Precision soil moisture measurement is important for water management, irrigation and crop planning. Soil moisture is one of the most important hydrological variables. This variable can be observable and it is essential not only for water management but also for climate prediction [1] Soil moisture measurement is also vital for many applications. Electronic devices, especially remote sensing from ground-based and space-based platforms for continuous monitoring of soil moisture, are widely used in order to improve irrigation management [2]. Soil moisture radiometer is a passive microwave device using to measure the amount of water in the soil. A radiometer measures the brightness temperature (T_B) of the soil by receiving thermal emission from the soil. The emissivity at the soil surface is directly related to the dielectric constant of soil, while dielectric constant is a function of volumetric soil moisture. Therefore, the measurement results of brightness temperature of the soil show the amount of water in it. Among the many possible frequency ranges, *L*-band frequency at 1.4 GHz is excellent for soil moisture measurement radiometer because of great penetration capability [1]. In a radiometer system, the fundamental parts are antenna system and a receiver module. Traditionally, horn antennas and reflector antennas are used due to their excellent radiation characteristics such as high gain and efficiency, low sidelobes and wide bandwidth. However, they are quite bulky and fixed beam hence requiring

The associate editor coordinating the review of this manuscript and approving it for publication was Feng Lin.

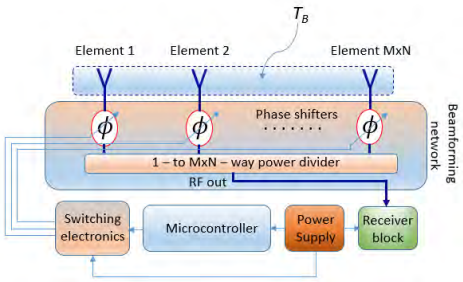

FIGURE 1. Block diagram of proposed L-band radiometer antenna.

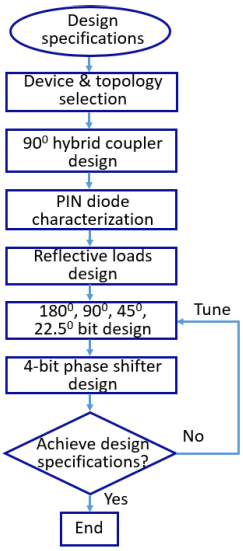

FIGURE 2. A 4-bit phase shifter design flow chart.

mechanical scanning. This work proposes an *L*-band patch antenna as an appropriate candidate for a radiometer system because of its planar configuration, compactness, low weight, low cost, and electronic scanning capability [3]–[5]. The configuration of the proposed *L*-band phased array antenna is shown in Figure 1.

Phase shifters are essential devices in many communications systems. A high-fidelity performance phase shifter is the one which has low insertion loss, high input and output return losses, a wide phase shifting range, and high phase resolution. In the phased array antenna system, phase shifters are the vital component for beamforming and 3D scanning. Phase shifters control the relative phase of individual radiating elements in a phased array to scan the beam. There are numerous discrete and Monolithic Microwave Integrated Circuit (MMIC) phase shifters including switched type [6]–[13], reflection-type [14]–[17], and vector sum method [18]–[20] reported recently. At low microwave frequency band such as *L*- and *S*-bands, the values of inductors, capacitors and physical size of transmission lines are quite large. Therefore, it is difficult to design these phase shifters on chip. Many designs of *L*- and *S*-band phase shifters have been implemented on Printed Circuit Board (PCB) using PIN diodes as switch elements [13], [21]–[24]. A PIN diode phase shifter using high-pass/low-pass topology provides low insertion loss and compact size but requires four PIN diodes for each bit [13]. Loaded line PIN diode phase shifter is suitable for small phase shift and also needs four PIN diodes for each bit [24]. Reflection type PIN diode phase shifter turns out to be promising since it needs only two PIN diodes per bit and provide excellent microwave performance. However, the disadvantage is the requirement of a hybrid coupler that makes the phase shifter large in size especially in the *L*-band. There are also some digital phase shifters at the *L*-band in the literature with low insertion loss and low RMS phase error; however, there is still a need for investigating and designing the phase shifter with new approach, low-cost solution, and compactness.

In this study, we propose the design of a low-cost, 4-bit digital, compact *L*-band reflection type PIN diode phase shifter with new, compact reflective loads and a compact meandered hybrid coupler. The cost of the phase shifter largely depends on the active device, in this case, the diode. A low-cost PIN diode is imperative because a beamforming network needs hundreds of them. We propose a low-cost band switching PIN diode BA682 from Philips, which cost only a couple of cents. But it has quite low off-state isolation making it a poor-quality switching element. The main reason is the high off-state capacitance of the diode. To overcome this problem, we consider a PIN diode as lumped components corresponding to forward and reverse states. Then, the loads are designed by adding only one inductor in parallel with the PIN diodes. By this approach, it is not necessary to have PIN diodes with high isolation. The designed phase shifter is a 4-bit type, providing 16 states of phase shifts with 22.5° resolution. The design procedure is as follows. First, we study the design specifications, select device and phase shifter topology. Next, we design the hybrid coupler, characterize the low-cost PIN diode and construct the equivalent circuits of PIN diode in reverse and forward bias states. Then, we analyze the reflective loads carefully and design the loads for different phase shift bit with least components for compactness. Finally, we design the phase shifters by employing quadrature hybrid couplers in conjunction with the reflective loads. The outcomes of the designed phase shifter are: (i) low insertion loss; (ii) low RMS phase error; and (iii) compact loads. The 4-bit phase shifter design flow chart is described in Figure 2.

This paper is organized as follows. Section II presents the theory of a reflection type phase shifter (RTPS) followed by its integration in a 4-bit PIN diode RTPS. Section III demonstrates the designs of meander branch-line 90° hybrid coupler. Section IV presents the PIN diode characterization using a transmission reflection through (TRL) calibration test fixture. The outcome is the extraction of the equivalent circuit model parameters in both on and off states. Then, the designs of the reflection loads are introduced and analyzed in Section V. Section VI presents the circuit design and fabrication of RTPS. Section VII presents the results and discussions followed by a conclusion in Section VIII.

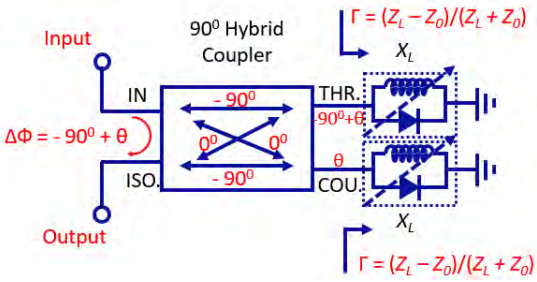

FIGURE 3. A single bit PIN diode RTPS with 90° hybrid coupler and reflective loads.

II. PROPOSED PIN DIODE PHASE SHIFTER

The schematic diagram of a single bit RTPS is demonstrated in Figure 3. It comprises a hybrid coupler with two reflective loads. The load is comprised of a PIN diode and an inductor in parallel as shown in the figure. The hybrid coupler divides the input signal into two equal amplitude signals but with a 90° phase shift at its through and couple ports. Assuming that the two reflective loads are identical, 90° coupler and the loads are lossless, the two reflected signals combine in-phase at the output, which is the isolation port. Meanwhile, the two reflected signals reach the input port with 180° out-of-phase; thus, they cancel each other. Assume that the phase shift caused by the loads is θ. The values of θ is negative if the load produces phase delay or positive if the load generates phase advance. Thus, the input signal comes in at the input port of coupler and goes out at the isolation port with the same amplitude, but with a phase shift of $\Delta\Phi$:

$$\Delta\Phi = -90^\circ + \theta \tag{1}$$

In this design, the loads are controlled by the band switching PIN diodes between forward and reverse bias states. When the diodes are forward biased, the phase shift at the output port is:

$$\Delta\Phi_f = -90^\circ + \theta_f \tag{2}$$

On the other hand, if the diodes are reverse biased:

$$\Delta\Phi_r = -90^\circ + \theta_r \tag{3}$$

The relative phase shift between forward and reverse bias states is:

$$\theta = \Delta\Phi_f - \Delta\Phi_r = \theta_f - \theta_r \tag{4}$$

Equation (4) shows that the phase shift of a single bit phase shifter solely depends on the relative phase difference of the load in its forward and reverse bias states. If the 90° coupler is well designed, the effects of coupler on the phase shift is insignificant. Therefore, the problem of achieving the phase shift of a single bit phase shifter is equivalently expressed as obtaining the phase shift of the reflective load. The detailed design of the reflective load will be presented in Section V. By cascading 22.5, 45, 90 and 180° phase shifter bits, the proposed 4-bit PIN diode RTPS as shown in Figure 4 is obtained.

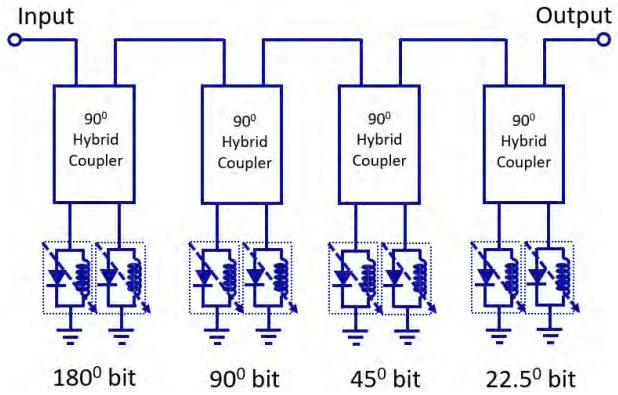

FIGURE 4. Proposed configuration of 4-bit PIN diode RTPS.

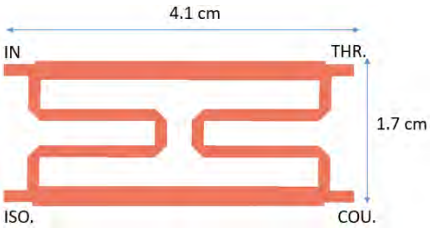

FIGURE 5. EM model of branch-line meandered 90° coupler.

III. DESIGNS OF COMPACT QUADRATURE HYBRID COUPLER

As stated above, the proposed RTPS will be used in the beamforming network of an L-band 4 × 4 element phased array radiometer antenna. Therefore, the compact design of the quadrature hybrid coupler is essential to accommodate the 16 phase shifters chain in the beamforming network. The meander branch-line coupler makes the proposed phase shifter a compact design. A quadrature hybrid coupler is a four-port passive device. There is one input port, two output ports and one isolated port. The amplitudes of signals at the two output are equal and the relative phase between the through and isolation ports is in quadrature. The EM model of the coupler is shown in Figure 5. To reduce the size, the 35 Ω microstrip line layout is drawn in meander style. The area of meandered branch-line coupler is 6.97 cm^2 while the area of the normal coupler is 15.17 cm^2. The designed coupler provides a 54 % of area reduction. In other words, the design only takes up 46% of the original size. The coupler is simulated in Keysight Advance Design System (ADS) Momentum suite and fabricated by using Taconic TLX8 substrate with the dielectric constant 2.55, thickness 0.5 mm, and copper thickness 17 microns.

IV. PIN DIODE CHARACTERIZATION

A. PIN DIODE CHARACTERISTICS

A PIN diode works as a current-controlled resistor at RF and microwave frequencies. The isometric view of a PIN diode is illustrated in Figure 6. There are three regions in a model of a PIN diode. They are heavily doped p^+ and n^+ regions

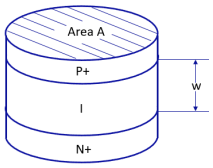

FIGURE 6. PIN diode structure.

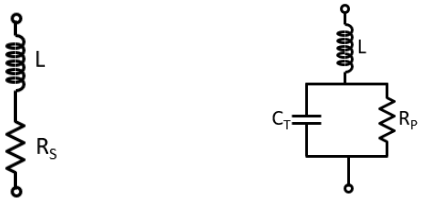

(a) (b)

FIGURE 7. PIN diode equivalent circuits: (a) forward bias and (b) reverse bias.

separated by a high resistance intrinsic layer (I). Due to random thermal motion, the diffusion of holes and electrons happens in the junctions between the intrinsic region and p^+ or n^+ regions, but the carriers cannot diffuse very far into I region. Therefore, with zero DC bias, the PIN diode is a non-conductive device. When the PIN diode is forward biased, the electric field injects holes and electrons into the I region. The charges do not recombine with each other instantaneously. The charges still exist for an average time, known as the carrier life time τ. This leads to the existence of storage charge. As a result, the intrinsic I region becomes a conductor. On the other hand, under reverse bias condition, both holes and electrons are swept out of the I region. There is no stored charge in the I region, and this makes PIN diode non-conductive [24]. The equivalent circuits of a diode in forward and reverse bias states are presented in Figure 7.

The equivalent circuit of the PIN diode is simplified as an inductor in series with a resistor when the PIN diode is forward biased. L is the parasitic inductance as a result of packaging. R_S is calculated as follows [24].

$$R_S = \frac{W^2}{2\mu \times Q} \tag{5}$$

where:

R_S = PIN diode forward resistance (Ω)
W = intrinsic I region width (cm)
μ = average carrier mobility (cm^2/V sec)
$Q = I_F \times \tau$ (stored charge, Coulombs)
I_F = forward bias current (A)
τ = average carrier lifetime (sec)

When the diode is reverse biased, the equivalent circuit is a parallel RC with a series L as shown in Figure 7(b). The value of R_P is proportional to reverse voltage. At RF and microwave frequencies, R_P is very large compared to the capacitance reactance; therefore, it is insignificant. The value of C_T is

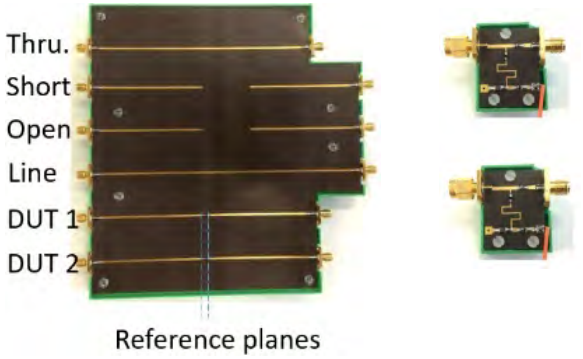

(a) (b)

FIGURE 8. (a) Test fixture and (b) bias T for diode characterization.

computed as follows.

$$C_T = \frac{\varepsilon A}{W} \tag{6}$$

where:

C_T = Reverse capacitance (F)
$\mathcal{E}$ = dielectric constant of silicon (F/m)
A = area of diode junction (m^2)
W = intrinsic I region width (m)

A good PIN diode has low R_S and small C_T so that it can provide low insertion loss when the diode is forward biased and high isolation when it is reverse biased. However, such diodes are expensive. This work used a very low-cost PIN diode which has large C_T. In the following section, the procedure of diode characterization is presented. Without proper characterization of PIN diode at design frequency we cannot achieve the design goal.

B. DESIGN OF TEST FIXTURE AND BIAS T

1) TEST FIXTURE

In order to characterize the diode, the TRL test fixture was designed. The photograph of the fabricated test fixture is shown in Figure 8(a). The calibration technique is TRL calibration, which is a 2-port calibration with three standards, thru (T), reflect (R), and line (L). All the lines in the text fixture have the same characteristics such as impedance, loss, and propagation; and only differ in length. The line length for the line standard is $\lambda/4$. The text fixture was simulated in ADS Momentum and fabricated by using Taconic TLX8 substrate.

2) BIAS T

The bias T network biases the PIN diode without letting DC current leaking into the network analyzer. The fabricated bias Ts are shown in Figure 8(b). The schematic of the designed bias T is shown in Figure 9. It is a three-port network where port 1 (P_1) is connected to the PIN diode, port 2 (P_2) is connected to the network analyzer, and port 3 (P_3) is connected to the DC supply. In the schematic, C_1 is a DC blocking capacitor, C_2 is a bypass capacitor, L_1 works as an RF choke, and R_1 is a current limiting resistor.

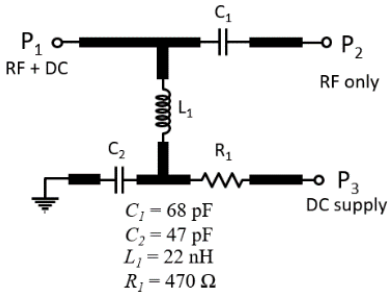

FIGURE 9. Schematic of designed bias T.

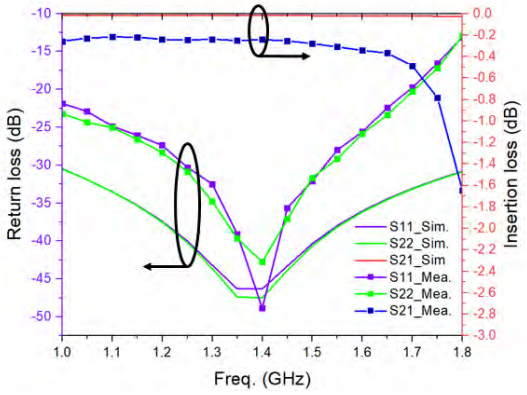

FIGURE 10. Insertion loss and return loss of bias T.

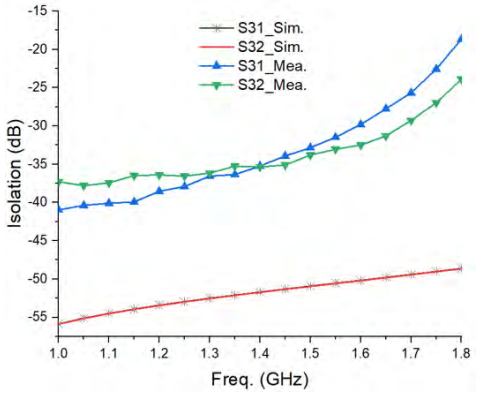

FIGURE 11. Isolation of bias T.

The simulation and measurement results of the bias T are shown in Figures 10 and 11. As can be seen in Figure 10, within 1.3 - 1.5 GHz bandwidth, in terms of measurement results, the return losses at port 1 and port 2 are larger than 30 dB, while the insertion loss between port 1 and port 2 is less than 0.25 dB. Regarding the isolation between port 3 (P_3) and two RF ports (P_1 and P_2), Figure 11 demonstrates more than 32 dB isolation. The measurement results are not as good as the simulation results due to the losses of the real components.

After designing the hardware, the standard definition file of the TRL calibration kits is edited and imported into Agilent E8361A performance network analyzer (PNA) for performing TRL calibration.

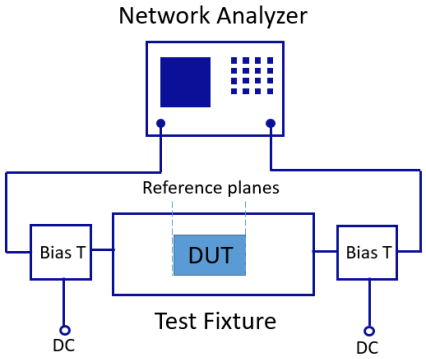

FIGURE 12. PIN diode characterization setup.

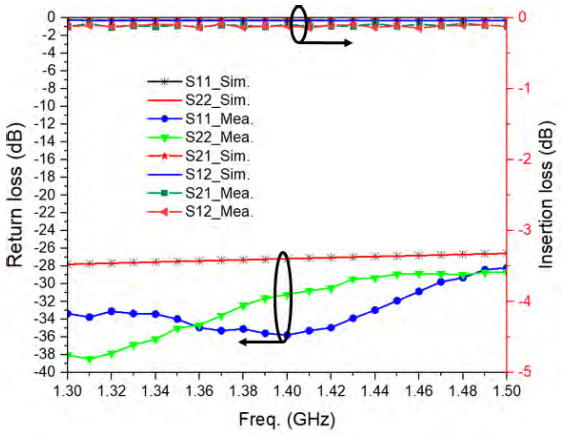

FIGURE 13. S-parameters of forward bias PIN diode.

C. PIN DIODE CHARACTERIZATION AND EQUIVALENT CIRCUITS

As stated before the low-cost PIN diode is a band switching PIN diode BA682 from Philips. In order to construct the equivalent circuits in forward and reverse states, the diode was characterized at a frequency range from 1.3 to 1.5 GHz using Agilent E8361A PNA, a TRL test fixture, and two bias-T networks. The PIN diode characterization setup is shown in Figure 12.

After performing TRL calibration, the reference planes are located at two ends of a device under test (DUT). In this design, for forward biasing, the PIN diode was characterized at 5 V with the forward bias current of 10 mA. For reverse biasing, the PIN diode was biased at 15 V. We characterized 5 PIN diodes. The *S*-parameters of the typical PIN diode in both forward and reverse states are shown in Figures 13 and 14 respectively. The measurement results revealed that the insertion loss in forward bias is quite small, and it is approximately about 0.1 dB. This indicates the small forward bias resistance R_S. However, in a reverse bias state, the isolation is poor, and it is just about 4 dB. We plotted the S-parameters on the Smith chart, by using the curve-fitting method, we obtained the equivalent circuit model parameters of the PIN diode, as shown in Figure 15. After constructing the equivalent circuits of the PIN diode, these models are

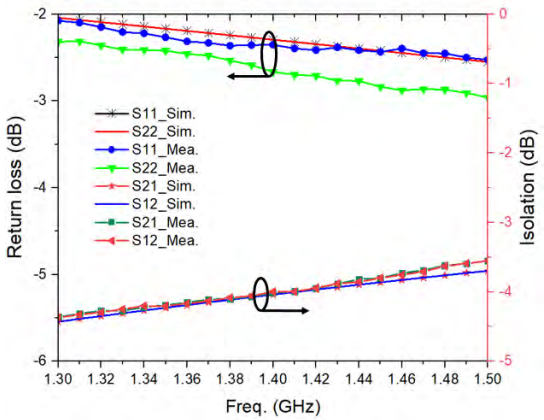

FIGURE 14. S-parameters of the reverse bias PIN diode.

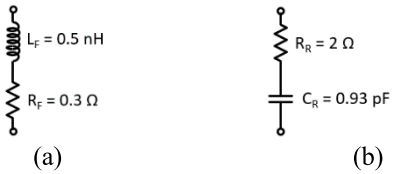

FIGURE 15. Simplified equivalent circuits of (a) forward bias and (b) reverse bias PIN diode.

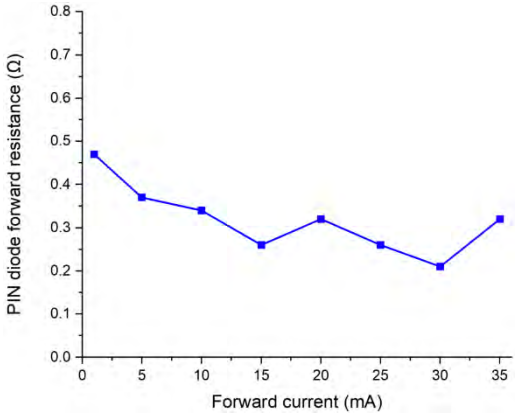

FIGURE 16. PIN diode forward resistance with various forward currents at 1.4 GHz.

simulated and the *S*-parameters in forward and reverse states are also plotted in Figures 13 and 14. As can be seen, there is good agreement between simulation and measurement results. This confirms the accuracy of the models. Trying to build the equivalent circuits corresponding to other measured PIN diodes, we found that the values of R_F, L_F, C_R are quite consistent. However, the value of R_R is ranging from 1 to 3 Ω. This value is insignificant compared to the reverse bias state capacitive reactance. Thus, the variation of the PIN diode does not affect the designed phase shifter performance significantly.

Choosing biasing voltage and current can affect the PIN diode performance. In forward bias, PIN diode forward resistance is a function of forward current. Large forward current results in small PIN diode forward resistance; however, the power consumption is large. Figure 16 illustrates the

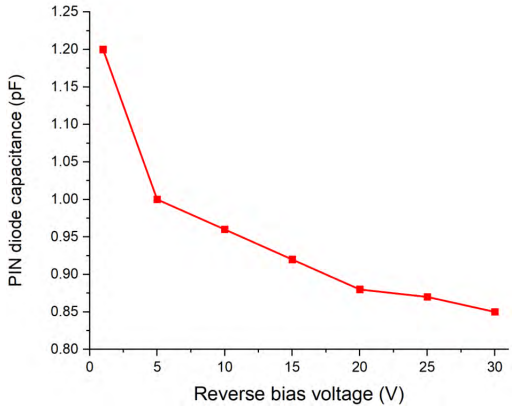

FIGURE 17. PIN diode capacitance with various reverse bias voltages at 1.4 GHz.

PIN diode forward resistance with various forward currents at 1.4 GHz. As can be seen, there is a downward trend of resistance when the forward current is increased. However, the values of resistance are just slightly changed with the range from 5 mA to 35 mA. Consequently, changing the forward current around 10 mA point does not affect the PIN performance significantly. In the reverse bias state, PIN diode capacitance is a function of reverse voltage. The high value of reverse voltage leads to small PIN diode capacitance. Figure 17 demonstrates the changing of PIN diode capacitance with various reverse bias voltages at 1.4 GHz. It is clear that changing the reverse bias around the 15 V point results in the change in PIN diode performance. Therefore, biasing PIN diodes with a precise voltage, especially in a reverse mode, is important to obtain the accurate phase shifts of the phase shifters.

V. DESIGNS OF THE REFLECTION LOADS

As discussed in Section II, the amount of phase shift in a load is equal to the phase shift in the output of a single bit phase shifter. In this section, we present the design of the loads to obtain 180°, 90°, 45°, and 22.5° phase shifts. As stated before, the ideal PIN diode behaves like a short circuit when it is forward biased and an open circuit when it is reverse biased. However, the measurement results in the previous section show the poor isolation in the reverse bias mode. Consequently, this kind of PIN diode cannot be used in conventional PIN diode phase shifters as presented in [25]. Our approach is that we consider the PIN diode as an inductor (0.5 nH) and a capacitor (0.93 pF) in forward and reverse bias respectively. The resistances in both forward and reverse bias states do not contribute significantly to the phase shifts; therefore, they are negligible in the calculations. By connecting the inductor in parallel with the diode, we calculate the values of inductance in order to obtain the desired phase shifts. With the case of 180° reflective load, in the reverse bias state, the load behaves like a capacitor. However, with 90°, 45°, 22.5° loads, also in the reverse bias state, the loads still act like inductors. Therefore, the calculations for designing two types of loads are presented in two different categories.

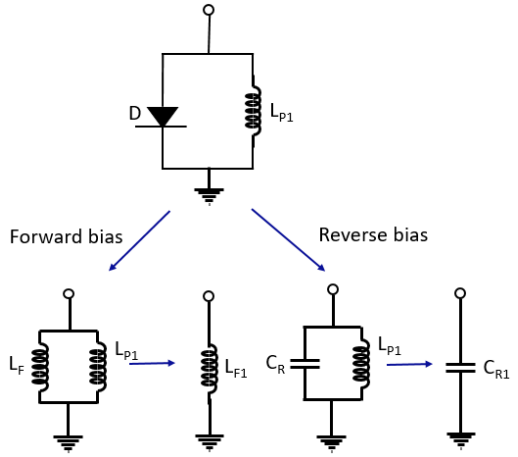

FIGURE 18. Simplified equivalent circuits of 180° bit in forward bias and reverse bias states.

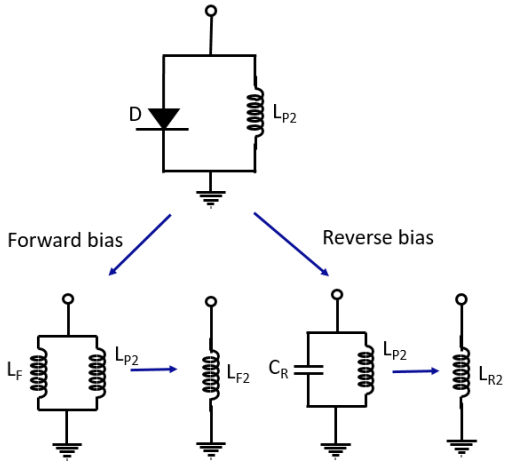

FIGURE 19. Simplified equivalent circuits of 90°, 45°, 22.5° bits in forward bias and reverse bias states.

A. DESIGN OF 180° REFLECTIVE LOAD

The simplified equivalent circuits of 180° bit in both forward bias and reverse bias states are shown in Figure 18. When the diode is forward biased, the reflection coefficients at the 180° reflective load are calculated as follows. When the diode is forward biased:

$$Z_{LF} = j\omega L_{F1} \tag{7}$$

$$\Gamma_{FB} = \frac{Z_{LF} - Z_0}{Z_{LF} - Z_0} \tag{8}$$

In which, Γ_{FB} is the reflection coefficient in the forward bias state. When the diode is reverse biased:

$$Z_{LR} = \frac{j\omega L_{P1}}{1 - \omega^2 L_{P1} C_R} \tag{9}$$

$$\Gamma_{RB} = \frac{Z_{LR} - Z_0}{Z_{LR} - Z_0} \tag{10}$$

In which, Γ_{RB} is the reflection coefficient in the reverse bias state. The phase shift is:

$$\theta_{180} = \angle\Gamma_{FB} - \angle\Gamma_{RB} \tag{11}$$

With the values of $L_F = 0.5$ nH, $C_R = 0.93$ pF, in order to achieve 180° phase shift, the value of L_{P1} is found as $L_{P1} = 18.08$ nH.

B. DESIGNS OF 90°, 45°, 22.5° REFLECTIVE LOADS

The simplified equivalent circuits of 90°, 45°, 22.5° bits in forward and reverse bias states are shown in Figure 19. In both states, the loads behave like inductors. The calculations of the values of inductors for 90°, 45°, 22.5° bits are performed by using (7) to (10). The inductance $L_{P2} = 4.5$ nH, $L_{P3} = 2.36$ nH, and $L_{P4} = 1.36$ nH are found as solutions for 90°, 45°, 22.5° loads respectively. The phase shift is:

$$\theta_{90\ or\ 45\ or\ 22.5} = \angle\Gamma_{RB} - \angle\Gamma_{FB} \tag{12}$$

The phase shifts for all the loads are presented on the Smith charts as shown in Figure 20.

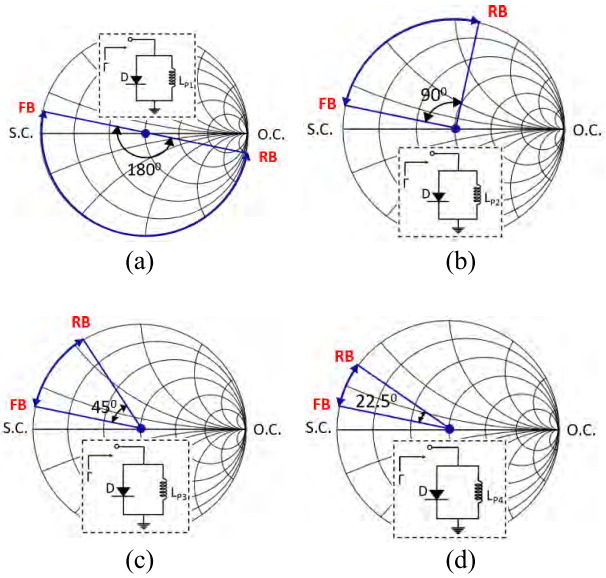

FIGURE 20. Phase shift trajectories of (a) 180°, (b) 90°, (c) 45°, (d) 22.5° reflective loads.

VI. CIRCUIT DESIGN AND FABRICATION

After making the calculations of the inductance in the loads, the layouts of 22.5°, 45°, 90°, 180° bit RTPS are drawn and simulated by using Keysight ADS Momentum. The photographs of the prototype 180°single bit and 4-bit RTPS are shown in Figure 21. In Figure 21(a), each bit phase shifter consists of a 90°-hybrid coupler and two identical loads. In the 180° reflective load, $C_1 = C_3 = 47$ pF are DC blocking capacitors; C_2=47 pF is a bypass capacitor;D is a PIN diode; $L_{P1} = 18$ nH is an inductor working with the diode for obtaining 180° phase shift; $L_1 = 56$ nH is an RF choke; R= 470 Ω is a current limiting resistor. The diode is controlled by bias voltages of 5 V/-15 V to drive the diode into forward and reverse bias states. In the cases of 22.5°, 45°, 90° bit RTPS, the inductance L_{P2}, L_{P3}, L_{P4} were realized by microstrip lines with different lengths.

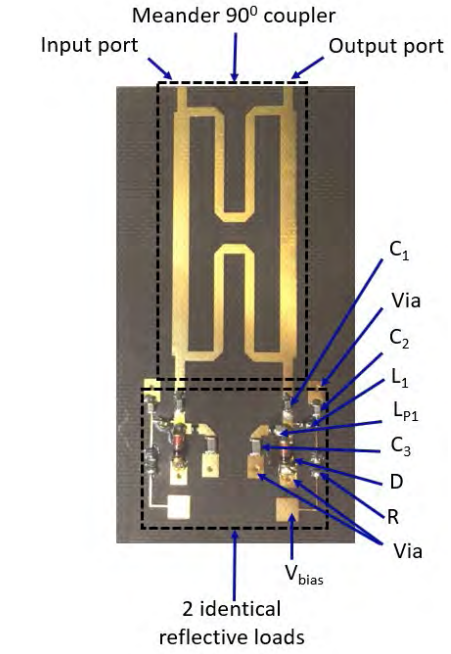

(a)

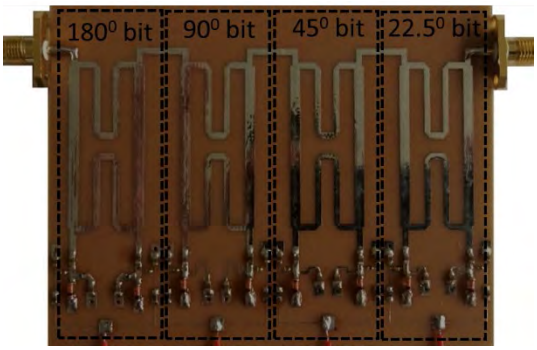

(b)

FIGURE 21. Photos of the fabricated (a) 180°-bit circuit and (b) 4-bit phase shifter.

After accomplishing the layouts of all the bits, the layout of 4-bit phase shifter is drawn cascading 4 individual bit circuits as shown in Figure 21(b). The size of 4-bit phase shifter is quite compact, just about 10 cm × 6 cm. After successful design and fabrication of the phase shifters, they we tested with AgilentE8361A PNA with appropriate bias states. The results are produced in the following section.

VII. RESULTS AND DISCUSSIONS

In this section, the simulated and measured results of the hybrid coupler and the phase shifter are presented. The measurements were performed with a full 2-port calibration on Agilent E8361A PNA in Monash Microwave, Antenna, RFID and Sensor Laboratory (MMARS) at Monash University.

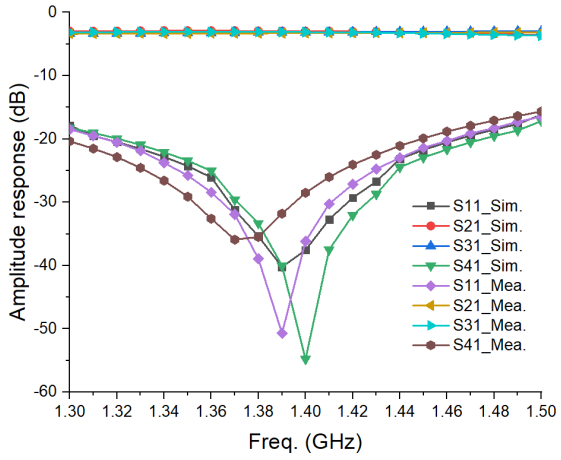

FIGURE 22. Amplitude response of meander branch-line 90° coupler.

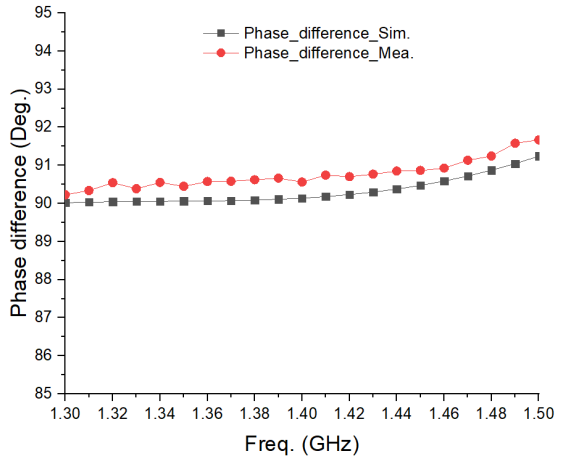

FIGURE 23. Phase response of meander branch-line 90° coupler.

A. 90° HYBRID COUPLER

The simulated and measured results of the coupler are shown in Figures 22 and 23. The results show that the designed coupler obtains very small amplitude imbalance and low insertion loss, which is just about 0.15 dB at 1.4 GHz. About the phase response, at 1.4 GHz, the phase difference between the through port and coupled port is about 90.5°. The measurement results indicate the excellent performance of the coupler. Figures 22 and 23 demonstrate good agreement between the simulated and measured results.

B. 4-BIT PHASE SHIFTER

The phase shifter was designed and simulated using Keysight ADS Momentum. The simulation results of the 4-bit phase shifter are shown in Figures 24, 25, and 26. The phase response in Figure 24 shows that at 1.4 GHz, the RMS phase error is almost zero.

The phase shifter behaves very well, except from the 180° phase state. The reason for that is only in180°-bit, the circuit works as a capacitance in reverse bias state while

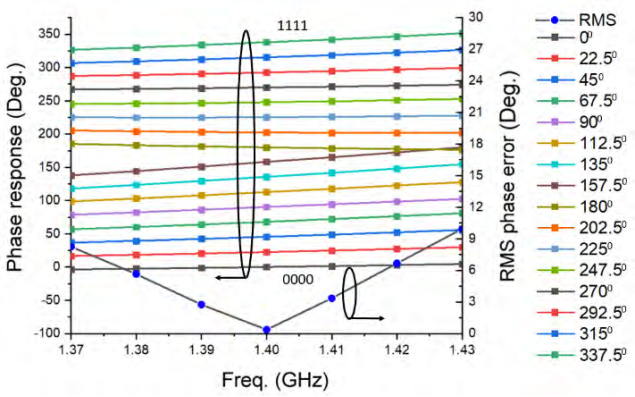

FIGURE 24. Simulated phase response of the phase shifter.

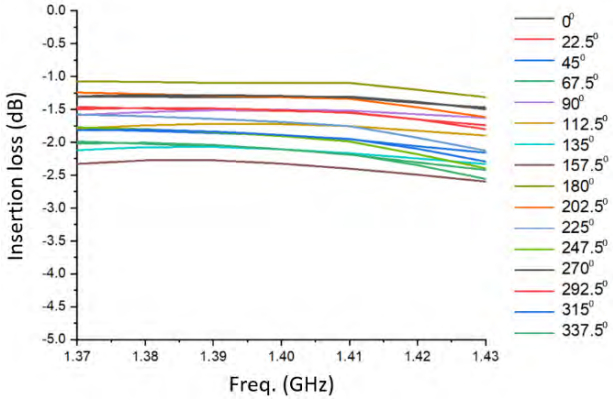

FIGURE 25. Simulated insertion loss of the phase shifter.

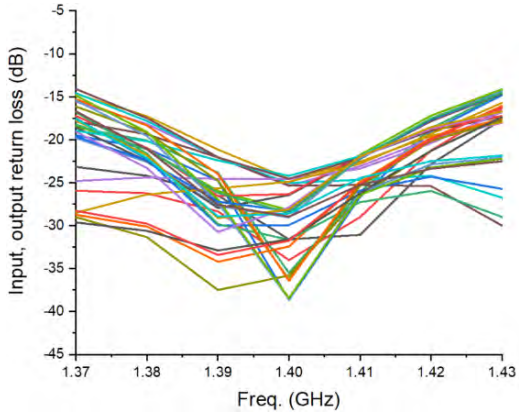

FIGURE 26. Simulated input and output return loss of the phase shifter.

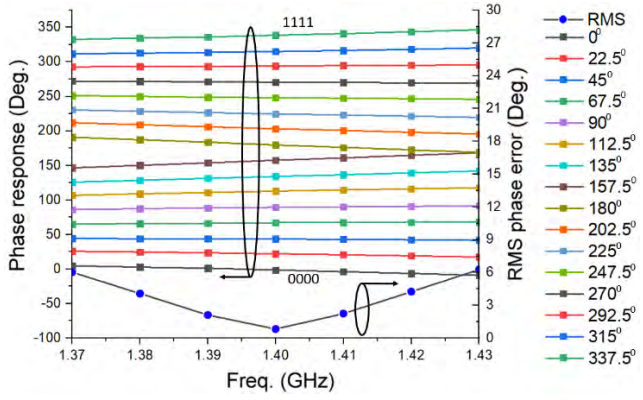

FIGURE 27. Measured phase response of the phase shifter.

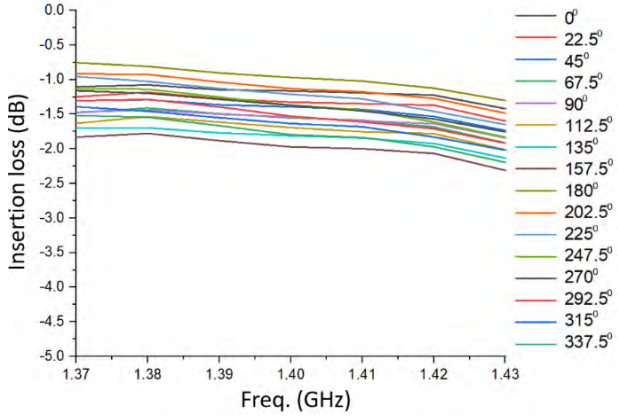

FIGURE 28. Measured insertion loss of the phase shifter.

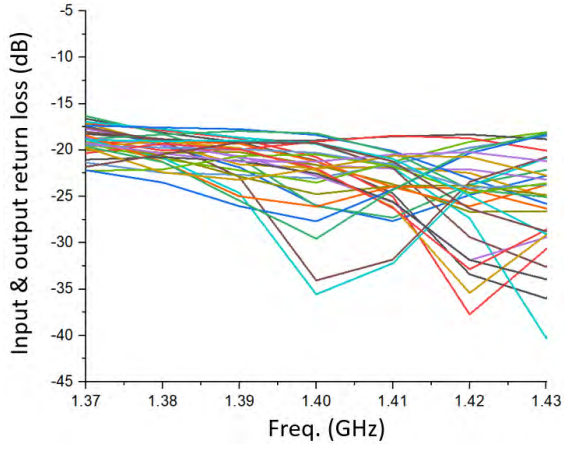

FIGURE 29. Measured input and output return loss of the phase shifter.

other bits perform as inductors in both forward and reverse states. In terms of amplitude response, Figure 25 illustrates the insertion loss of phase shifter in 16 phase states. The insertion loss is ranging from 1 to 2.4 dB within the bandwidth from 1.37 to 1.43 GHz. Figure 26 reveals that the phase shifter can obtain the return losses more than 14 dB within 1.37 to 1.43 GHz bandwidth in all phase shift states.

The measurement results of the prototype 4-bit phase shifter are shown in Figures 27 to 29. The switching operation of the PIN diode is performed by altering the bias voltage V_{bias} = 5 V/-15 V. When the PIN diode is forward biased, with the use of the current limiting resistor R = 470 Ω, the on-state DC current is about 10 mA. The reverse bias state of the PIN diode is driven by the V_{bias} = 15 V. The measured phase performance of the 4-bit phase shifter from 1.37 to 1. 43 GHz is shown in Figure 27.

The RMS phase error within the radiometer bandwidth (25 MHz, 1.8%) is less than 3°. At the center frequency

TABLE 1. Performance comparison of the proposed phase shifter with other works.

Ref.	Tech-nology	Freq. (GHz)	Bit	RMS Phase Error (^{0})	IL (dB)	RL (dB)
[13]	HP/LP PIN diode, PCB	2.4 - 2.5	4	< 4.1	8.8	13
[26]	HP/LP MMIC	1.4 - 2.4	4	< 3	3.2	10
[27]	TL, SW PCB	1.0 - 2.0	4	< 3.6	4.0	12
[28]	PIN diode PCB	2.0 - 4.0	4	< 6	12.5	10
[29]	HP/LP MMIC	2.7 - 3.5	6	<1	5	15
[30]	HP/LP, BP, AP PCB	0.53 - 1.1	4	<6	2.5	13
This work	**PIN diode PCB**	**1.37 - 1.43**	**4**	**< 6 1 @1.4 GHz**	**2.3**	**16**

of 1.4 GHz, the measured RMS phase error is very small, which is just less than 1°. In terms of amplitude response, the fabricated 4-bit phase shifter achieves a very small insertion loss, which is just less than 2 dB within the 25 MHz bandwidth and less than 2.3 dB from 1.37 to 1.43 GHz, as shown in Figure 28. As revealed in Figure 29, the return losses higher than 16 dB are obtained for all states from 1.37 to 1.43 GHz. Compared to the simulation results, the measurement results quite agree with the simulation results, with slightly better performance in both phase and amplitude responses. The maximum power consumption of the phase shifter is about 400 mW when all the bits are on-state. In short, the phase shifter obtained excellent performance.

Comparison with reported works: Table 1 shows a comparative study of the work with the reported works on the L-band phase shifter. As can be seen, the prototype is superior in performance compared to the reported work. The superiority comes in the bandwidth, better insertion and return losses and phase shift performance.

VIII. CONCLUSION

A high performance 1.4 GHz *L*-band phase shifter based on low-cost PIN diodes was analyzed, fabricated and tested. The diode was characterized with the state-of-the-art in house developed TRL calibration jig and Agilent E8216 PNA at the designed frequency band. The curve fitting technique of the measured *S*-parameter data of the diode helps to construct the accurate equivalent circuits of the low-cost commercial PIN diode. A compact reflective load is designed by adding only one inductor. The compactness of the signal bit phase shifter is further enhanced with the meandered line hybrid coupled that yield 54% reduction of size. Finally, the L-band 4-bit phase shifter was designed successfully with the tandem of four individual bits. The fabricated 4-bit phase shifter showed the very small RMS phase error, just less than 1°, at center frequency 1.4 GHz. Also, the phase shifter obtained the small insertion loss of less than 2 dB within radiometer 25 MHz bandwidth and return loss larger than 16 dB for the bandwidth from 1.37 to 1.43 GHz. The excellent performance phase shifter will be integrated into an *L*-band phased array antenna for soil moisture radiometer.

ACKNOWLEDGMENT

The authors would like to thank the Australian Government for providing Endeavour PhD Scholarship.

REFERENCES

[1] T. J. Jackson, "Measuring surface soil moisture using passive microwave remote sensing," *Hydrol. Processes*, vol. 7, no. 2, pp. 139–152, 1993.
[2] L. Hassan-Esfahani, A. Torres-Rua, and M. McKee, "Assessment of optimal irrigation water allocation for pressurized irrigation system using water balance approach, learning machines, and remotely sensed data," *Agricult. Water Manage., Article*, vol. 153, pp. 42–50, May 2015.
[3] K. Carver and J. Mink, "Microstrip antenna technology," *IEEE Trans. Antennas Propag.*, vol. AP-29, no. 1, pp. 2–24, Jan. 1981.
[4] F. Yang, X.-X. Zhang, X. Ye, and Y. R. Samii, "Wide-band E-shaped patch antennas for wireless communications," *IEEE Trans. Antennas Propag.*, vol. 49, no. 7, pp. 1094–1100, Jul. 2001.
[5] F. Babaeian and N. C. Karmakar, "A high gain dual polarized ultra-wideband array of antenna for chipless RFID applications," *IEEE Access*, vol. 6, pp. 73702–73712, 2018.
[6] W.-T. Li, Y.-C. Chiang, J.-H. Tsai, H.-Y. Yang, J.-H. Cheng, and T.-W. Huang, "60-GHz 5-bit phase shifter with integrated VGA phase-error compensation," *IEEE Trans. Microw. Theory Techn.*, vol. 61, no. 3, pp. 1224–1235, Mar. 2013.
[7] J.-H. Tsai, C.-K. Liu, and J.-Y. Lin, "A 12 GHz 6-bit switch-type phase shifter MMIC," in *Proc. 44th Eur. Microw. Conf.*, 2014, pp. 1916–1919.
[8] Q. Zheng, Z. Wang, K. Wang, G. Wang, H. Xu, L. Wang, W. Chen, M. Zhou, Z. Huang, and F. Yu, "Design and performance of a wideband Ka-band 5-b MMIC phase shifter," *IEEE Microw. Wireless Compon. Lett.*, vol. 27, no. 5, pp. 482–484, May 2017.
[9] I. J. Bahl and D. Conway, "*L*- and *S*-band compact octave bandwidth 4-bit MMIC phase shifters," *IEEE Trans. Microw. Theory Techn.*, vol. 56, no. 2, pp. 293–299, Feb. 2008.
[10] G.-S. Shin, J.-S. Kim, H.-M. Oh, S. Choi, C. W. Byeon, J. H. Son, J. H. Lee, and C.-Y. Kim, "Low insertion loss, compact 4-bit phase shifter in 65 nm CMOS for 5G applications," *IEEE Microw. Wireless Compon. Lett.*, vol. 26, no. 1, pp. 37–39, Jan. 2016.
[11] S. Dey, S. K. Koul, A. K. Poddar, and U. L. Rohde, "Reliable and compact 3- and 4-bit phase shifters using MEMS SP4T and SP8T switches," *J. Microelectromech. Syst.*, vol. 27, no. 1, pp. 113–124, Feb. 2018.
[12] B.-W. Min and G. M. Rebeiz, "Single-ended and differential Ka-band BiCMOS phased array front-ends," *IEEE J. Solid-State Circuits*, vol. 43, no. 10, pp. 2239–2250, Oct. 2008.
[13] M. T. Qureshi, V. Desmaris, M. Geurts, and J. van de Sluis, "Passive reciprocal high-pass/low-pass 4-bit phase shifter at 2.45 GHz," in *Proc. 44th Eur. Microw. Conf.*, 2014, pp. 1076–1078.
[14] J. C. Wu, T. Y. Chin, S. F. Chang, and C. C. Chang, "2.45-GHz CMOS reflection-type phase-shifter MMICs with minimal loss variation over quadrants of phase-shift range," *IEEE Trans. Microw. Theory Techn.*, vol. 56, no. 10, pp. 2180–2189, Oct. 2008.
[15] R. Garg and A. S. Natarajan, "A 28-GHz low-power phased-array receiver front-end with 360° RTPS phase shift range," *IEEE Trans. Microw. Theory Techn.*, vol. 65, no. 11, pp. 4703–4714, Nov. 2017.
[16] P. Gu and D. Zhao, "Ka-band CMOS 360° reflective-type phase shifter with ±0.2 dB insertion loss variation using triple-resonating load and dual-voltage control techniques," in *Proc. IEEE Radio Freq. Integr. Circuits Symp. (RFIC)*, Jun. 2018, pp. 140–143.
[17] A. Natarajan, A. Valdes-Garcia, B. Sadhu, S. K. Reynolds, and B. D. Parker, "W-band dual-polarization phased-array transceiver front-end in SiGe BiCMOS," *IEEE Trans. Microw. Theory Techn.*, vol. 63, no. 6, pp. 1989–2002, Jun. 2015.
[18] K.-J. Koh and G. M. Rebeiz, "0.13-μm CMOS phase shifters for X-, Ku-, and K-band phased arrays," *IEEE J. Solid-State Circuits*, vol. 42, no. 11, pp. 2535–2546, Nov. 2007.

[19] I. Kalyoncu, E. Ozeren, A. Burak, O. Ceylan, and Y. Gurbuz, "A phase-calibration method for vector-sum phase shifters using a self-generated LUT," *IEEE Trans. Circuits Syst. I, Reg. Papers*, vol. 66, no. 4, pp. 1632–1642, Apr. 2019.
[20] B. Cetindogan, E. Ozeren, B. Ustundag, M. Kaynak, and Y. Gurbuz, "A 6 bit vector-sum phase shifter with a decoder based control circuit for X-band phased-arrays," *IEEE Microw. Wireless Compon. Lett*, vol. 26, no. 1, pp. 64–66, Jan. 2016.
[21] P. Srinivasa, A. K. Singh, A. Sharma, and S. K. Koul, "Design of a novel S band dual mode low loss high power PIN diode phase shifter with planar folded dipole configuration," in *Proc. IEEE Int. Conf. Microw., Commun., Antennas Electron. Syst. (COMCAS)*, Nov. 2011, pp. 1–4.
[22] J. Komisarezuk, "Four bit phase shifter for the L band," in *Proc. 12th Int. Conf. Microw. Radar. Conf. (MIKON)*, vol. 2, 1998, pp. 590–594.
[23] N. C. Karmakar and M. E. Bialkowski, "Low cost phase shifters for L-band phased array antennas," in *IEEE Antennas Propag. Soc. Int. Symp. Dig.*, vol. 4, Jul. 1997, pp. 2476–2479.
[24] J. F. White, "Diode phase shifters for array antennas," *IEEE Trans. Microw. Theory Techn.*, vol. MTT-22, no. 6, pp. 658–674, Jun. 1974.
[25] D. M. Pozar, *Microwave Engineering*, 4th ed. Hoboken, NJ, USA: Wiley, 2011, p. 752.
[26] Q. Xiao, "A compact L-band broadband 4-bit MMIC phase shifter with low phase error," in *Proc. Asia–Pacific Microw. Conf.*, 2011, pp. 291–294.
[27] X. Tang and K. Mouthaan, "Phase-shifter design using phase-slope alignment with grounded shunt λ/4 stubs," *IEEE Trans. Microw. Theory Techn.*, vol. 58, no. 6, pp. 1573–1583, Jun. 2010.
[28] E. Erkek and Ş. Demir, "S-band hybrid 4 bit phase shifter," in *Proc. 10th Medit. Microw. Symp.*, 2010, pp. 40–43.
[29] D. L. Allen and T. Nguyen, "Compact phase accurate low loss s-band 6-bit phase shifter in a 5×5 mm^2 plastic over molded package," in *Proc. IEEE Compound Semiconductor Integr. Circuit Symp. (CSICS)*, Oct. 2016, pp. 1–4.
[30] X. Tang and K. Mouthaan, "Design considerations for octave-band phase shifters using discrete components," *IEEE Trans. Microw. Theory Techn.*, vol. 58, no. 12, pp. 3459–3466, Dec. 2010.

KIM TUYEN TRINH (S'16) received the B.E. degree in telecommunications engineering from Telecommunications University (TCU), Vietnam, in 2002, and the M.E. degree in telecommunications engineering from La Trobe University, VIC, Australia, in 2012. He is currently pursuing the Ph.D. degree in electrical engineering with Monash University, Australia. His research interests include antennas and propagation, phase shifters, phased array antennas, and mobile networks.

JIEWEI FENG (S'16) received the Diploma of Engineering from Monash College, in 2010, and the Bachelor of Engineering (Hons.) in electrical and computer system and the Master of Advanced Engineering in electrical engineering from Monash University, in 2015 and 2016, respectively, where he is currently pursuing the Ph.D. degree in high resolution soil moisture remote sensing. His research interests include microstrip patch antenna, phased array, and radiometer receiver design.

SHAHRIAR HASAN SHEHAB (S'19) received the B.Sc. Engg. degree in electrical and electronics engineering and the M.Sc. Engg. degree in electrical and electronics engineering from American International University-Bangladesh (AIUB), Bangladesh, in 2013 and 2014, respectively. He is currently pursuing the Ph.D. degree with Monash Microwave, Antennas, RFID and Sensors research group, Monash University, Australia. His research interests include substrate integrated waveguide technology, phased array antennas, and satellite communications.

NEMAI CHANDRA KARMAKAR (S'91–M'91–SM'99) received the M.Sc. degree in electrical engineering from the University of Saskatchewan, Saskatoon, SK, Canada, in 1991, and the Ph.D. degree from The University of Queensland, Brisbane, QLD, Australia, in 1999. He has over 20 years of teaching, design, and development experience in antennas, microwave active and passive circuits, and RFIDs in Canada, Australia, and Singapore. He is currently an Associate Professor with the Department of Electrical and Computer Systems Engineering, Monash University, Melbourne, VIC, Australia. He has authored or coauthored over 220 referred journal and conference papers, 24 book chapters, and 8 books. He holds nine international patent applications on chipless RFID.